THE JOURNAL OF PHYSICAL CHEMISTRY B

Article

pubs.acs.org/JPCB

Understanding the Binding Mechanism of Various Chiral SWCNTs and ssDNA: A Computational Study

Siamkhanthang Neihsial,[†] Ganga Periyasamy,[†] Pralok K. Samanta,[†] and Swapan K. Pati*[,†,‡]

[†]Theoretical Sciences Unit and [‡]New Chemistry Unit, Jawaharlal Nehru Center for Advanced Scientific Research, Jakkur P.O., Bangalore 560064, India

Supporting Information

ABSTRACT: Molecular dynamics (MD) simulations have been carried out to understand the binding mechanism of various chiral single-walled carbon nanotubes (SWCNTs) and single-stranded DNA (ssDNA) of four different nucleobase sequences (i.e., $ssdA_{14}$, $ssdT_{14}$, $ssdG_{14}$, and $ssdC_{14}$, where, A, T, G, and C are adenine, thymine, guanine, and cytosine, respectively) in aqueous media at room temperature (300 K) and atmospheric pressure (1 atm). The simulations studies reveal that ssDNA undergoes rapid structural changes and wrap around the SWCNTs via π-stacking interactions between SWCNT's wall and the nucleobases of ssDNA. Our computations demonstrate that the length of the ssDNA plays an important role during the wrapping process. Moreover, it suggests that the length of the sequence should be proportional to the diameter of the SWCNT, in order to overcome the intralocked π-stacking interactions between the nucleobases of ssDNA sequence. Also, in our classical MD simulation, we do not observe the correlation between the diameter of SWCNTs and the sequences of ssDNA, which indicates the importance of electronic factors of these systems. In order to understand the electronic contributions of these systems, the quantum calculations have been performed at Hartree−Fock level for the 17 ns MD simulated structures. The quantum chemical calculations provide evidence that the highly stable ssDNA@SWCNT hybrid possesses a larger HOMO−LUMO gap.

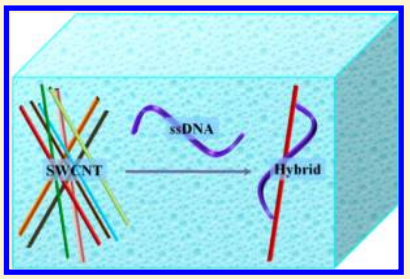

1. INTRODUCTION

Single-walled carbon nanotubes (SWCNTs)[1] are tubular nanostructures, which possess a wide spectrum of applications in various research fields, such as optoelectronics,[2,3] sensing,[4,5] molecular electronics,[6,7] and biomedicines,[8,9] because of its outstanding mechanical, electronic, and optical properties.[10] SWCNTs are conceptualized by wrapping a graphene sheet into a hollow cylinder[10] and having a covalently bonded sp^2 carbon. The rolling up of graphene sheet to form SWCNT is represented by the chiral vectors (n,m), where n and m are integers. SWCNTs can be metallic, semiconducting or moderate semiconducting. and even insulating depending on their chiral vectors.[11,12]

Most of the applications of SWCNT, such as conductive films,[13,14] high-performance field-effect transistor,[15] nanoscale sensor,[16] and optical devices[17] require a population of SWCNT with identical chirality, which is difficult to obtain using current synthetic methods.[18] Thus, intense efforts have been put in to advance the techniques for separating single chiral SWCNTs from its synthetic mixture,[19] which are dielectrophoresis,[20] selective oxidation,[21] electrical breakdown,[22] ultracentrifugation,[23,24] and deoxyribonucleic acid (DNA) wrapping chromatography.[8,9,25,26] Among these methods, separation of identical chiral SWCNTs via DNA wrapping chromatography has generated a great deal of interest among the scientific community. In fact, DNA is a flexible, amphiphilic genetic material,[27] and its electronic nature can be tuned easily by changing its nucleobase sequences.[28−32] The effective and facile nature of single-strand DNA (ssDNA) makes it a more powerful candidate to wrap a SWCNT than the double strand DNA (dsDNA), which needs vigorous sonication[25] in the latter case. There are theoretical[33−42] and experimental[41,43−51] studies devoted to the understanding of the interaction between ssDNA and SWCNT, which concluded that the π-stacking and some van der Waals (vdW) interactions between the components are the driving force for its wrapping[33−36] mechanism. Moreover, the interactions between a few chiral SWCNT and ssDNA sequences have been studied experimentally to elucidate their selectivity nature.[43−47] However, the reason and mechanisms behind the chiral specificity of ssDNA toward the SWCNTs have barely been explored. Mostly, it is decided based on trial and error method. Hence, a systematic and general study is required to understand the interaction between each and every single chiral SWCNT with various ssDNA sequences. Exploring the thermodynamics and kinetics of the DNA wrapping process is difficult to achieve via experimental methods, whereas computational studies will provide more information at low cost. Since the high level quantum chemical calculations are computationally very expensive for these types of systems, molecular dynamics (MD) simulations are used for detailed understanding of these processes.[33−36]

Received: June 15, 2012
Revised: November 29, 2012
Published: November 30, 2012

To efficiently and systematically explore the sequence of ssDNA for the separation of a specific SWCNT, we have examined four polynucleotide sequences of adenine ($ssdA_{14}$), thymine ($ssdT_{14}$), guanine ($ssdG_{14}$), and cytosine ($ssdC_{14}$). Moreover, various chiral SWCNTs are considered, which are (5,5), (6,5), (6,6), (8,0), (9,0), and (9,3) SWCNTs.

2. COMPUTATIONAL DETAILS

MD simulations are carried out by considering infinite length neutral SWCNTs of chiral vectors of (9,3), (9,0), (8,0), (6,6), (6,5), and (5,5) at 300 K temperature and 1 atm pressure. To obtain the microscopic picture of the ssDNA specificity toward the SWCNT, MD simulations are performed by considering $ssdG_{14}$, $ssdA_{14}$, $ssdC_{14}$, and $ssdT_{14}$ discrete strands. The ssDNAs are created using nab (nucleic acid builder) module implemented in the Amber 11 Tools Package.[52] The length of the sequence was premeditated based on the previous MD studies on (11,0) SWCNT.[53] The AMBER99 force fields[54] are used to model ssDNA. The SWNTs' carbon atoms are modeled as uncharged Lennard-Jones particles (using sp^2 parameters from the AMBER99) as reported in the literature.[55,56] The negatively charged backbones of ssDNA are neutralized using Na^+ counterions. The transferable intermolecular potential three point (TIP3P) model[57] is considered for water as the solvent. All the MD simulations are performed using GROMACS 4.0.7 Simulations Package[58] in an initial cubic water box of 8.00 Å × 8.00 Å × *Lz* Å (where, *Lz* = 12.33 for (11,0), (9,0), and (8,0) SWCNTs; 12.03 for (6,6) and (5,5) SWCNTs; 12.27 for (9,3) SWCNT; and 12.17 for (6,5) SWCNT) at constant temperature (300 K)[59] and constant pressure (1 atm).[60] Periodic boundary condition (PBC) was applied in all the three directions. The initial configurations for the hybrid simulations are created by stretching, straightening the ssDNA, and keeping the sequences at ∼13.0 Å away from SWCNTs (see unbound state in Figure 1).[53] Moreover, the

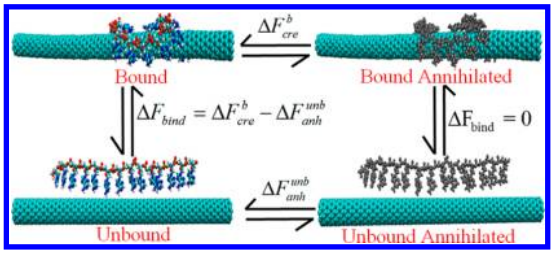

Figure 1. Schematic representation of the thermodynamic cycle used for free energy computations. All the configurations are surrounded by the cubic box of water molecules.

nucleobases are considered to be pointing toward the SWCNT. The high energy contacts between the atoms in the initial conformations of SWCNT, ssDNA, and the hybrid systems are removed by minimizing the energy using the steepest decent integration method. Following that, MD simulations are performed using leapfrog algorithm for integrating Newton's equation of motion for 17 ns at constant temperature (300 K) and pressure (1 bar). The time scale is reasonable with the reported MD simulation for nonperturbed initial configuration, which was in the range of 3 to 20 ns by various research groups for similar kinds of systems.[38,39,41,42] Moreover, we have carried out a 40 ns simulation for (9,0), (9,3), and (5,5) SWCNTs with the four ssDNA sequences in order to validate our time scale. Electrostatic interactions are calculated with the Particle Mesh Ewald (PME) method.[61] In order to obtain a clear picture about the mechanism, the position of SWCNT atoms are constrained with a harmonic potential throughout the MD simulations as reported in the previous MD studies.[35,53] The time step for the MD simulation is 1.5 fs, and the atomic coordinates are recorded at every 7.5 ps for trajectory analysis. Analysis and visualization of MD trajectories are performed with VMD software.[62] The interaction energies are Lennard-Jones (LJ) energies, which are calculated by averaging throughout the trajectory between the corresponding fragments.

Thermodynamics integration (TI)[63] method as implemented in the GROMACS-4.0.7 MD package[58] is employed to compute the binding free energies between the ssDNA and SWCNT by introducing various coupling parameters (λ) in the Hamiltonian (H). On the basis of previous studies",[64] the change in binding free energies (ΔF_{bind}) are calculated by considering a thermodynamics cycle as shown in Figure 1. ΔF_{bind} is defined as the free energy difference between the bound and unbound states.

$$\Delta F_{bind} = \Delta F^{b}_{cre} - \Delta F^{unb}_{anh}$$

where ΔF^{b}_{cre} (ΔF^{unb}_{anh}) is the change in free energy (ΔF) to create (annihilate) ssDNA in the bound (unbound) states. To compute theΔF, vdW interactions are annihilated/created using λ values of 0.00, 0.25, 0.50, 0.75, and 1.00. Soft-core LJ potentials are employed with soft-core parameter $\alpha = 0.5$ and λ power, $p = 1$. At each λ value, $(\delta H/\delta\lambda)$ is extracted from the 17 ns trajectory.

In order to understand the contribution of electronic factors in the binding interaction, single-point Hartree−Fock (HF) quantum chemical calculations have been performed with minimal STO-3G basis set as implemented in the Gaussian09 package.[65] Note that, it would be very expensive to do calculations for these systems with a high level of methods and/or basis sets. For the HF calculations, the Na^+ and water molecules are removed from the final geometry of 17 ns MD simulation. The nonperiodic passivated edges of SWCNTs are considered. The negatively charged ssDNA are neutralized by protonating one of the two oxygen atoms in the phosphate group.[66]

3. RESULTS AND DISCUSSION

The wrapping of DNA on SWCNT in aqueous media can be visualized by two simple steps; the first step entails solvation of ssDNA, and the second step consists of the wrapping process of ssDNA on SWCNT. An understanding of each step is indispensable to acquire the complete mechanism of this process.

3.1. ssDNA in Aqueous Media. The ssDNA molecule is flexible in bond torsional angles within the dinucleotide levels as well as in the sugar−phosphate backbone. Each ssDNA is solvated in water at 300 K with 1 atm pressure in order to study its dynamics. Our studies show that the ssDNA interacts with water via strong H-bonding network (0.25−0.30 nm distance and 165−175° of ∠D···H···A, where D and A are donor and acceptor, respectively).[67] Among the four, $ssdG_{14}$ forms stronger H-bond networks with water (170 average numbers of H-bonds) and thereby results in the larger solvation energy (−60.33 cal mol^{-1}). The exposure of three H-bonding modes of $ssdG_{14}$ (−60.33 kcal mol^{-1}) and $ssdC_{14}$ (−54.69 kcal mol^{-1}) to water is the reason for its higher interaction energy with

dx.doi.org/10.1021/jp305894c | J. Phys. Chem. B 2012, 116, 14754−14759

water than the $ssdA_{14}$ (−45.01 kcal mol^{-1}) and $ssdT_{14}$ (−36.96 kcal mol^{-1}). In addition, the larger surface area of $ssdG_{14}$ makes the sequence to interrelate more with water than the $ssdC_{14}$. The above studies clearly elucidate intermolecular interactions between ssDNA and the aqueous media. Now, it is apparent that the both intramolecular π-stacking between the nucleobases in the sequence and H-bonds with solvent energy barriers have to be defeated in order to wrap the ssDNA over the SWCNTs.

3.2. SWCNTs in Aqueous Media. Although pure SWCNTs are hydrophobic in nature, it is crucial to understand its interaction with water media. In the initial configuration, the water molecules inside the SWCNT are removed for all cases, which is necessary condition for SWCNT in aqueous medium.[53] The simulations are performed for 17 ns, which showed that the (9,3), (9,0), (8,0), (6,6), (6,5), and (5,5) chiral SWCNTs are extremely stable (Figure 2). This is in agreement with the previous results on SWCNT (11,0).[53,68]

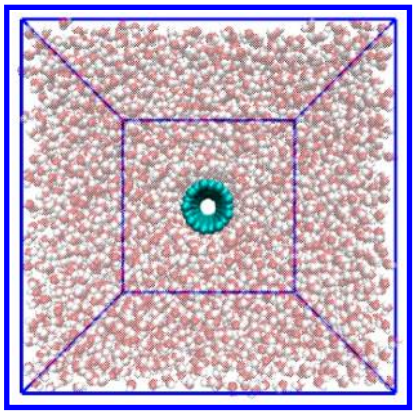

Figure 2. Shown is the 17 ns MD simulated structure of (9,0) SWCNT at 300 K. Note that the complete structure is oriented to show the hollow space in SWCNT.

Although the SWCNTs considered in our study are hydrophobic in nature, they are coupled to water via weak interactions with their surfaces. These interactions vary according to the diameters. Six different chiral SWCNTs are considered with various diameters to recognize the size-dependent behavior of SWCNTs toward water, which are 0.63 (8,0), 0.68 (5,5), 0.70 (9,0), 0.77 (6,5), 0.81 (6,6), and 0.84 nm (9,3). The computed interaction energies between the neutral SWCNTs and water molecules are directly proportional to the SWCNTs diameter. The SWCNT and solvent interaction energy order is (in units of kcal mol^{-1}) −609 (8,0) < −644 (5,5) < −653 (9,0) < −690 (6,5) < −731 (6,6) < −739 (9,3). The interaction energy indicates the stability of SWCNT in water with the hollow sphere, and the amount of interaction energy is directly proportional to the exposure of the SWCNT surface to the water.

3.3. Structure of ssDNA−SWCNT Hybrid. The hybrid simulation is very complicated and needs a systematic study to obtain a complete wrapping mechanism. At the starting point, the straight ssDNA is placed ∼13.0 Å away from the SWCNT. This will be helpful to realize the preferential geometry assumed by the ssDNA upon binding to SWCNT during the course of MD simulation. Our computation shows that, around 0.1 ns, the ssDNA start to wrap around the SWCNTs by breaking its natural self π-stacking interactions between the nucleobases and few intermolecular H-bonding networks with water, which prolongs for 5−6 ns. After 5−6 ns, it attains a complete bound state. For example, the snapshots during the MD simulation between $ssdA_{14}$ and (9,0) SWCNT are given in Figure 3. However, the simulations are carried out for 17 ns, where the fluctuations in total energies are negligible (see Figure S1, Supporting Information, for total energy landscape). Note, we are aware that the time scale is not enough to obtain complete statistics of these systems. However, we believe that this time scale is enough to describe at least the qualitative trend of these systems. Furthermore, we have validated the time scale by extending up to 40 ns for (9,3), (9,0), and (5,5) SWCNTs with four ssDNA sequences (see Figure S2, Supporting Information), where we have not observed any change in their interaction energy order. This study shows that the ssDNA interact with SWCNT via π-stacking interactions as reported in the previous theoretical[33−36] studies. Time-dependent simulation provides evidence that the phosphate and sugar backbones change their orientations in various manners in order to formulate the ssDNA in perfect orientation with large π-stacking interaction with SWCNT as shown in the Figure 4.

3.3.1. Diameter-Dependent Wrapping. In general, irrespective of the diameters, the adsorption of nucleotide chains is largely complete within the 5 ns of simulation time, where the π-stacking interaction among the nucleobases of an ssDNA is entirely vanished. Note that the time scale is shorter than others because of the initial preferred configurations. However, the orientation of ssDNA differs based on its diameter. The simulation shows that the ssDNA enfolded on smaller diameter SWNTs possess a more intralocked H-bonding network within the nucleobases than in higher diameter wrapped ssDNA (see

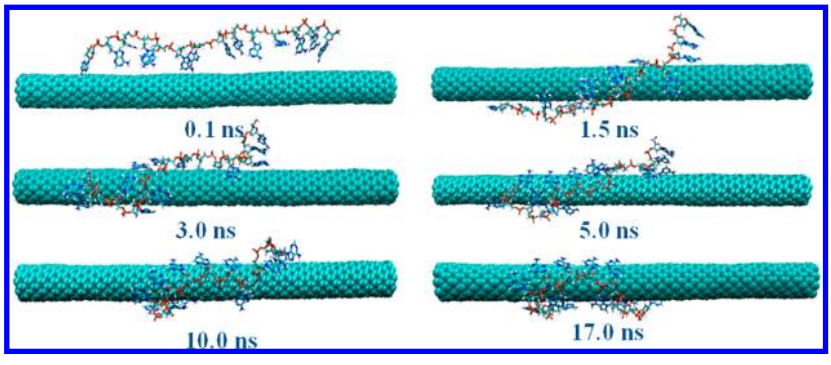

Figure 3. Various snapshots of $ssdA_{14}$@(9,0) SWCNT hybrid configurations during the 17 ns MD simulation at constant temperature (300 K) and pressure (1 atm).

dx.doi.org/10.1021/jp305894c | J. Phys. Chem. B 2012, 116, 14754−14759

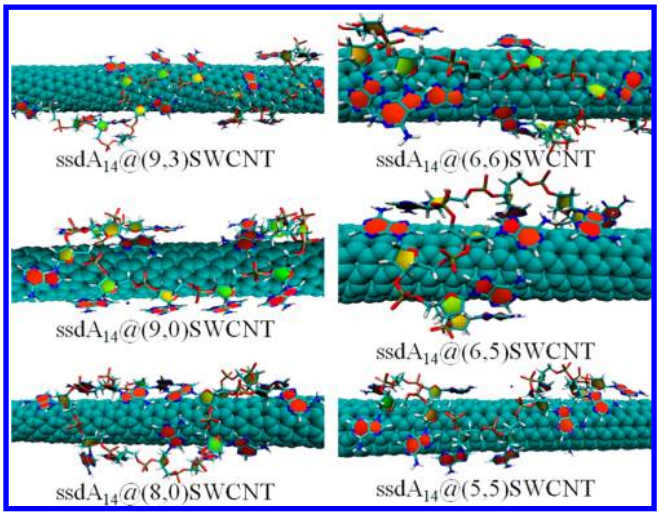

Figure 4. MD simulated structure of ssdA$_{14}$@(n,m) SWCNT composite. Note that the hybrid zones are enlarged to show the orientation of DNA scaffolds (sugar, phosphate, and nuclobases) in order to form perfect π-stacking.

Figure 4). The numbers of intralocked H-bonds are given in the Table 1. From Table 1, it is evident that intralocked H-bonds within the sequence are inversely proportional to its diameter. For example, the smaller diameter SWCNTs ((5,5) and (8,0)) possess more intralocked H-bonds than larger diameter SWCNTs. Moreover, the wrapping decreases the exposure of ssDNA toward water. Our studies show that the change in the helical conformation of ssDNA during the SWCNT wrapping process increases the number of intralocked H-bonds and decreases the H-bond interaction with water. In addition, the above-mentioned results provide the evidence that the ssDNA length is playing an important role in the wrapping mechanism. Moreover, in the MD simulation, we did not observe the correlation between the diameter and sequence selectivity, where the similar diameter follows the different trend (see Table 2). However, it can be attributed to their electronic properties.

Table 1. Average Total Number of H-Bonds (within 3.5 Å) within ssDNA and between the Water and ssDNA Throughout the 17 ns MD Simulation; Diameters (nm) of the SWCNTs Are Also Given (in italic)

systems			
chirality of SWCNT	ssDNA	average number of intralocked H-bonding interaction within ssDNA	average number of H-bonds between ssDNA and water
without SWCNT	ssdA14		157
	ssdG14		172
	ssdC14		162
	ssdT14		146
(8,0)	ssdA14	2	157
0.63	ssdG14	10	161
	ssdC14	6	145
	ssdT14	2	141
(5,5)	ssdA$_{14}$	2	152
0.68	ssdG$_{14}$	9	162
	ssdC$_{14}$	6	147
	ssdT$_{14}$	2	141
(9,0)	ssdA$_{14}$	2	150
0.70	ssdG$_{14}$	6	161
	ssdC$_{14}$	5	155
	ssdT$_{14}$	2	139
(6,5)	ssdA$_{14}$	2	151
0.77	ssdG$_{14}$	6	163
	ssdC$_{14}$	5	153
	ssdT$_{14}$	2	139
(6,6)	ssdA$_{14}$	1	150
0.81	ssdG$_{14}$	5	163
	ssdC$_{14}$	3	148
	ssdT$_{14}$	1	139
(9,3)	ssdA$_{14}$	0	153
0.84	ssdG$_{14}$	5	164
	ssdC$_{14}$	3	150
	ssdT$_{14}$	1	139

Table 2. Binding Free Energies (ΔF_{bind}, in kcal mol^{-1}) between Various ssDNA and SWCNTs; the Orders of Binding Free Energy against the Nanotubes are also given; the HOMO−LUMO Energy Gaps (in eV) of the Hybrids are also written in the parentheses

SWCNTs	ssdA$_{14}$ (A)	ssdT$_{14}$ (T)	ssdG$_{14}$ (G)	ssdC$_{14}$ (C)	order
(9,3)	−19.21	−19.84	−20.90	−25.54	C > G > T > A
	(1.06)	(1.10)	(1.22)	(1.32)	
(9,0)	−43.45	−25.87	−54.46	−67.39	C > G >A > T
	(0.55)	(0.30)	(1.22)	(1.33)	
(8,0)	−24.77	−16.67	−12.66	−13.55	A > T > C > G
	(1.59)	(1.10)	(0.28)	(0.41)	
(6,6)	−34.98	−16.57	−28.05	−17.03	G > A >C > T
	(1.45)	(1.41)	(1.46)	(1.42)	
(6,5)	−58.00	−23.41	−18.01	−29.70	A > C > T > G
	(2.69)	(2.49)	(2.31)	(2.57)	
(5,5)	−19.50	−15.37	−30.72	−12.94	G > A > T > C
	(1.66)	(1.53)	(1.75)	(1.55)	

Though the electronic factors are not included in the simulation, we have observed group dependent behavior, which is given in Table 2. MD simulations show that the (5,5) and (6,6) SWCNTs prefer to bind with ssdG$_{14}$ more than any other nucleobase sequences as observed in previous tight binding model calculations between CNT and polymer DNA.[69] The computed interaction energies are in the following order ssdG$_{14}$ > ssdA$_{14}$ > ssdC$_{14}$ ≈ ssdT$_{14}$. Similarly, (8,0) and (6,5) SWCNTs favor to bind with ssdA$_{14}$ than ssdT$_{14}$, ssdC$_{14}$, and ssdG$_{14}$. The computed order of interaction energy for (6,5) SWCNT is comparable with the reported experimental findings and order based on MD simulation results of dinucleotide and (6,5) SWCNT.[70] Moreover, SWCNTs (9,0) and (9,3) like to bind with the ssdC$_{14}$ base as in tight binding model calculations between CNT and polymer DNA[69] rather than ssdA$_{14}$, ssdG$_{14}$, and ssdT$_{12}$, where the observed trend is ssdC$_{14}$ > ssdG$_{14}$ > ssdA$_{12}$ ≈ ssdT$_{12}$ sequences.

3.3.2. Quantum Chemical Calculations. The above-mentioned MD results illustrate that there could be a correlation between electronic nature and the sequence selection. In order to understand it, single-point quantum mechanical calculations have been carried out at HF level, using the minimal STO-3G basis set. The quantum chemical calculations provide evidence that the hybrid with higher binding energy possess larger HOMO (highest occupied molecular orbital)−LUMO (lowest unoccupied molecular

dx.doi.org/10.1021/jp305894c | J. Phys. Chem. B 2012, 116, 14754−14759

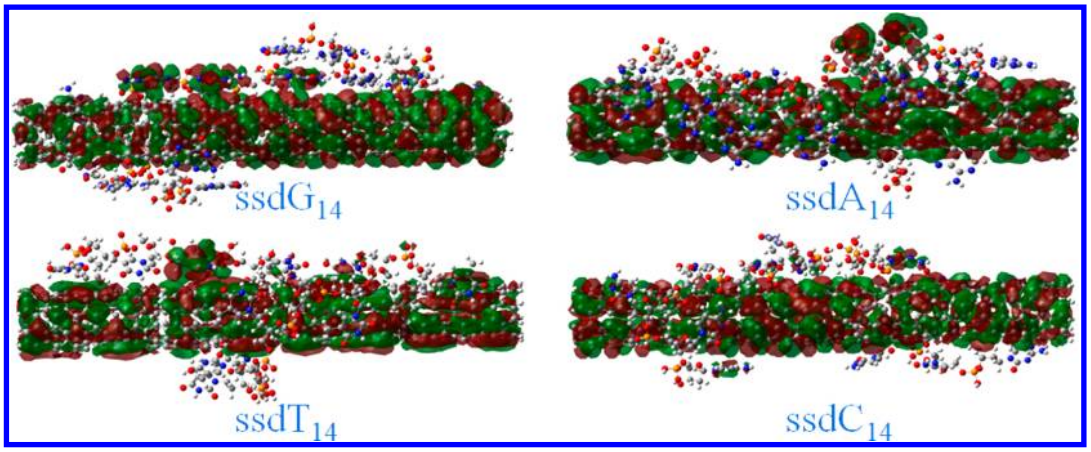

Figure 5. Computed highest energy delocalized frontier MOs (where the ssDNA start to contribute) of various ssDNA@(5,5) SWCNT hybrids. The isocontour value of 0.002 electron/Bohr^3 is used for plotting. The variations in the ssDNA contributions are shown.

orbital) gap. For a single chiral SWCNT, the ssDNA sequence, which results in a larger HOMO−LUMO gap, forms a chemically more stable ssDNA@SWCNT hybrid. The computed MO shows that there is a delocalization between SWCNT and ssDNA in the hybrid, where the amount of delocalization varies depending on the sequence in the hybrid. The hybrid with the larger delocalization makes it to be chemically more stable with larger HOMO−LUMO gap. Herein, we show the highest energy MOs for ssDNA@(5,5) SWCNT hybrid (see Figure 5) as an example. The larger amount of delocalization in the ssdG_{14}@(5,5) SWCNT hybrid is the reason for its higher binding free energy than the ssdA_{14}@(5,5) SWCNT, ssdT_{14}@(5,5) SWCNT, and ssdC_{14}@(5,5) SWCNT systems. These calculated quantum chemical results hint that the electronic delocalization between ssDNA and SWCNT correlate with each other for selectively. This proves the contribution of electronic factors in the sequence selectivity.

4. CONCLUSIONS

Using MD simulations, the binding free energies between the 14-nucleobase ssDNA (ssdA_{14}, ssdT_{14}, ssdG_{14}, and ssdC_{14}) over several SWCNTs have been carried out up to 17 ns (and 40 ns for a few systems). Our computations provide the evidence for the stability of SWCNT in the water environment at room temperature and atmospheric pressure. Our MD simulation shows that the ssDNA changes its geometrical orientation in order to achieve perfect π-stacking interaction between ssDNA and SWCNT. In addition, our studies demonstrate the correlation between the length of the ssDNA and SWCNT diameter. The length of the sequence should be inversely proportional to the diameter of the SWCNT, to overcome the internal π-stacking interactions between the nucleobases in ssDNA. Moreover, our results provide evidence that the electronic factors of the hybrid determine the sequence selectivity. The quantum mechanical studies at the HF level show that the wrapping makes the system chemically more stable with a larger HOMO−LUMO gap. This occurs due to larger delocalization of MOs over ssDNA and SWCNT in the ssDNA@SWCNT hybrid.

■ ASSOCIATED CONTENT

Supporting Information

Interaction energy between the different SWCNT and ssDNA in the time scale of 17 ns. Interaction energy between the (9,3), (9,0), and (5,5) SWCNTs and ssDNA in the time scale of 40 ns. This material is available free of charge via the Internet at http://pubs.acs.org.

■ AUTHOR INFORMATION

Corresponding Author

*E-mail: pati@jncasr.ac.in.

Notes

The authors declare no competing financial interest.

■ ACKNOWLEDGMENTS

G.P. is thankful for the DST-Women scientist fellowship, and P.K.S. thanks CSIR (Govt. of India) for a research fellowship. S.K.P. acknowledges DST (Government of India) and AOARD, US Air Force, for a research grant.

■ ABBREVIATIONS USED

MD, molecular dynamics; SWCNT, single-walled carbon nanotube; ssDNA, single-stranded DNA; HF, Hartree−Fock

■ REFERENCES

(1) Dresselhaus, M. S.; Dresselhaus, G.; Avouris, P. *Carbon Nanotubes Synthesis, Structure, Properties, and Applications*; Springer: New York, 2001; Vol. *80*.

(2) Hatton, R. A.; Miller, A. J.; Silva, S. R. P. *J. Mater. Chem.* **2008**, *18*, 1183−1192.

(3) Misewich, J. A.; Martel, R.; Avouris, P.; Tsang, J. C.; Heinze, S.; Tersoff, J. *Science* **2003**, *300*, 783−786.

(4) Heller, I.; Janssens, A. M.; Mannik, J.; Minot, E. D.; Lemay, S. G.; Dekker, C. *Nano Lett.* **2008**, *8*, 591−595.

(5) Kong, J.; Franklin, N. R.; Zhou, C. W.; Chapline, M. G.; Peng, S.; Cho, K. J.; Dai, H. J. *Science* **2000**, *287*, 622−625.

(6) Borghetti, J.; Derycke, V.; Lenfant, S.; Chenevier, P.; Filoramo, A.; Goffman, M.; Vuillaume, D.; Bourgoin, J. P. *Adv. Mater.* **2006**, *18*, 2535−2540.

(7) Chen, J.; Perebeinos, V.; Freitag, M.; Tsang, J.; Fu, Q.; Liu, J.; Avouris, P. *Science* **2005**, *310*, 1171−1174.

(8) Kostarelos, K.; Lacerda, L.; Pastorin, G.; Wu, W.; Wieckowski, S.; Luangsivilay, J.; Godefroy, S.; Pantarotto, D.; Briand, J. P.; Muller, S.; Prato, M.; Bianco, A. *Nat. Nanotechnol.* **2007**, *2*, 108−113.

(9) Zhang, Y. B.; Kanungo, M.; Ho, A. J.; Freimuth, P.; van der Lelie, D.; Chen, M.; Khamis, S. M.; Datta, S. S.; Johnson, A. T. C.; Misewich, J. A.; Wong, S. S. *Nano Lett.* **2007**, *7*, 3086−3091.
(10) Saito, R.; Dresselhaus, G.; Dresselhaus, M. S. *Physical Properties of Carbon Nanotubes*; Imperial College Press: London, U.K., 1999.
(11) Haddon, R. C. *Acc. Chem. Res.* **2002**, *35*, 997−997.
(12) Niyogi, S.; Hamon, M. A.; Hu, H.; Zhao, B.; Bhowmik, P.; Sen, R.; Itkis, M. E.; Haddon, R. C. *Acc. Chem. Res.* **2002**, *35*, 1105−1113.
(13) Green, A. A.; Hersam, M. C. *Nano Lett.* **2008**, *8*, 1417−1422.
(14) Wu, Z. C.; Chen, Z. H.; Du, X.; Logan, J. M.; Sippel, J.; Nikolou, M.; Kamaras, K.; Reynolds, J. R.; Tanner, D. B.; Hebard, A. F.; Rinzler, A. G. *Science* **2004**, *305*, 1273−1276.
(15) Javey, A.; Guo, J.; Wang, Q.; Lundstrom, M.; Dai, H. J. *Nature* **2003**, *424*, 654−657.
(16) Barone, P. W.; Baik, S.; Heller, D. A.; Strano, M. S. *Nat. Mater.* **2005**, *4*, 86−92.
(17) Weisman, R. B. *Anal. Bioanal. Chem.* **2010**, *396*, 1015−1023.
(18) Sinha, N.; Yeow, J. T. W. *IEEE Trans. Nanobiosci.* **2005**, *4*, 180−195.
(19) Tu, X.; Manohar, S.; Jagota, A.; Zheng, M. *Nature* **2009**, *460*, 250−253.
(20) Krupke, R.; Hennrich, F.; von Lohneysen, H.; Kappes, M. M. *Science* **2003**, *301*, 344−347.
(21) Miyata, Y.; Kawai, T.; Miyamoto, Y.; Yanagi, K.; Maniwa, Y.; Kataura, H. *J. Phys. Chem. C* **2007**, *111*, 9671−9677.
(22) Collins, P. C.; Arnold, M. S.; Avouris, P. *Science* **2001**, *292*, 706−709.
(23) Arnold, M. S.; Green, A. A.; Hulvat, J. F.; Stupp, S. I.; Hersam, M. C. *Nat. Nanotechnol.* **2006**, *1*, 60−65.
(24) Yanagi, K.; Miyata, Y.; Kataura, H. *Appl. Phys. Express* **2008**, *1*, 34003.
(25) Zheng, M.; Jagota, A.; Semke, E. D.; Diner, B. A.; McLean, R. S.; Lustig, S. R.; Richardson, R. E.; Tassi, N. G. *Nat. Mater.* **2003**, *2*, 338−342.
(26) Zheng, M.; Semke, E. D. *J. Am. Chem. Soc.* **2007**, *129*, 6084−6085.
(27) Saenger, W. *Principles of Nucleicd Acid Structure*; Springer-Verlag: New York, 1984.
(28) Mallajosyula, S. S.; Lin, J. C.; Cox, D. L.; Pati, S. K.; Singh, R. R. P. *Phys. Rev. Lett.* **2008**, *101*, 176805.
(29) Senthilkumar, K.; Grozema, F. C.; Guerra, C. F.; Bickelhaupt, F. M.; Lewis, F. D.; Berlin, Y. A.; Ratner, M. A.; Siebbeles, L. D. A. *J. Am. Chem. Soc.* **2005**, *127*, 14894−14903.
(30) Iliafar, S.; Wagner, K.; Manohar, S.; Jagota, A.; Vezenov, D. V. *J. Phys. Chem. C* **2012**, *116*, 13896−13903.
(31) Manohar, S.; Mantz, A. R.; Bancroft, K. E.; Hui, C. Y.; Jagota, A.; Vezenov, D. V. *Nano Lett.* **2008**, *8*, 4365−4372.
(32) Cathcart, H.; Nicolosi, V.; Hughes, J. M.; Blau, W. J.; Kelly, J. M.; Quinn, S. J.; Coleman, J. N. *J. Am. Chem. Soc.* **2008**, *130*, 12734−12744.
(33) Enyashin, A. N.; Gemming, S.; Seifert, G. *Nanotechnology* **2007**, *18*, 245702.
(34) Johnson, A. T. C.; Staii, C.; Chen, M.; Khamis, S.; Johnson, R. R.; Klein, M. L.; Gelperin, A. *Phys. Status Solidi B* **2006**, *243*, 3252−3256.
(35) Johnson, R. R.; Johnson, A. T. C.; Klein, M. L. *Small* **2010**, *6*, 31−34.
(36) Roxbury, D.; Jagota, A.; Mittal, J. *J. Am. Chem. Soc.* **2011**, *133*, 13545−13550.
(37) Zhao, X. *J. Phys. Chem. C* **2011**, *115*, 6181−6189.
(38) Cheng, C. L.; Zhao, G. J. *Nanoscale* **2012**, *4*, 2301−2305.
(39) Roxbury, D.; Manohar, S.; Jagota, A. *J. Phys. Chem. C* **2012**, *114*, 13267−13276.
(40) Wang, Y. *J. Phys. Chem. C* **2008**, *112*, 14297−14305.
(41) Zhao, X.; Johnson, J. K. *J. Am. Chem. Soc.* **2007**, *129*, 10438−10445.
(42) Martin, W.; Zhu, W.; Krilov, G. *J. Phys. Chem. B* **2008**, *112*, 16076−16089.
(43) Chen, Y.; Liu, H.; Ye, T.; Kim, J.; Mao, C. *J. Am. Chem. Soc.* **2007**, *129*, 8696−8697.
(44) Gigliotti, B.; Sakizzie, B.; Bethune, D. S.; Shelby, R. M.; Cha, J. N. *Nano Lett.* **2006**, *6*, 159−164.
(45) Gladchenko, G. O.; Karachevtsev, M. V.; Leontiev, V. S.; Valeev, V. A.; Glamazda, A. Y.; Plokhotnichenko, A. M.; Stepanian, S. G. *Mol. Phys.* **2006**, *104*, 3193−3201.
(46) Singh, P.; Kumar, J.; Toma, F. M.; Raya, J.; Prato, M.; Fabre, B.; Verma, S.; Bianco, A. *J. Am. Chem. Soc.* **2009**, *131*, 13555−13562.
(47) Kim, S. N.; Kuang, Z.; Grote, J. G.; Farmer, B. L.; Naik, R. R. *Nano Lett.* **2008**, *8*, 4415−4420.
(48) Roxbury, D.; Mittal, J.; Jagota, A. *Nano Lett.* **2012**, *12*, 1464−1469.
(49) Roxbury, D.; Tu, X.; Zheng, M.; Jagota, A. *Langmuir* **2011**, *27*, 8282−8293.
(50) Karachevtsev, M. V.; Karachevtsev, V. A. *J. Phys. Chem. B* **2011**, *115*, 9271−9279.
(51) Albertorio, F.; Hughes, M. E.; Golovchenko, J. A.; Branton, D. *Nanotechnology* **2009**, *20*, 395101.
(52) Case, D. A.; Darden, D. A.; Cheatham, T. E., III; Simmerling, C. L.; Wang, J.; Duke, R. E.; Luo, R.; Walker, R. C.; Zhang, W.; Merz, K. M.; et al. *AMBER11*; University of California: San Francisco, CA, 2010.
(53) Johnson, R. R.; Johnson, A. T. C.; Klein, M. L. *Nano Lett.* **2008**, *8*, 69−75.
(54) Cornell, W. D.; Cieplak, P.; Bayly, C. I.; Gould, I. R.; Merz, K. M.; Ferguson, D. M.; Spellmeyer, D. C.; Fox, T.; Caldwell, J. W.; Kollman, P. A. *J. Am. Chem. Soc.* **1995**, *117*, 5179−5197.
(55) Hummer, G.; Rasaiah, J. C.; Noworyta, J. P. *Nature* **2001**, *414*, 188−190.
(56) Zou, J.; Ji, B. H.; Feng, X. Q.; Gao, H. J. *Nano Lett.* **2006**, *6*, 430−434.
(57) Jorgensen, W. L. *J. Am. Chem. Soc.* **1981**, *103*, 335−340.
(58) Hess, B.; Kutzner, C.; van der Spoel, D.; Lindahl, E. *J. Chem. Theory Comput.* **2008**, *4*, 435−447.
(59) Bussi, G.; Donadio, D.; Parrinello, M. *J. Chem. Phys.* **2007**, *126*, 7.
(60) Berendsen, H. J. C.; Postma, J. P. M.; van Gunsteren, W. F.; Dinola, A.; Haak, J. R. *J. Chem. Phys.* **1984**, *81*, 3684−3690.
(61) Darden, T.; York, D.; Pedersen, L. *J. Chem. Phys.* **1993**, *98*, 10089−10092.
(62) Humphrey, W.; Dalke, A.; Schulten, K. *J. Mol. Graphics Modell.* **1996**, *14*, 33−38.
(63) Chipot, C.; Pohorille, A. *Free Energy Calculations: Theory and Applictions in Chemistry and Biology*; Springer: Berlin, Germany, 2007.
(64) Samanta, P. K.; Periyasamy, G.; Manna, A. K.; Pati, S. K. *J. Mater. Chem.* **2012**, *22*, 6774−6781.
(65) Frisch, M. J.; Trucks, G. W.; Schlegel, H. B.; Scuseria, G. E.; Robb, M. A.; Cheeseman, J. R.; Scalmani, G.; Barone, V.; Mennucci, B.; Petersson, G. A.; et al. *Gaussian 09*, revision A.1 Gaussian, Inc.: Wallingford, CT, 2009.
(66) Churchill, C. D. M.; Wetmore, S. D. *Phys. Chem. Chem. Phys.* **2011**, *13*, 16373−83.
(67) Neihsial, S.; Lyngdoh, R. H. D. *J. Comput. Chem.* **2008**, *29*, 1788−1797.
(68) Lemasson, F. A.; Strunk, T.; Gerstel, P.; Hennrich, F.; Lebedkin, S.; Barner-Kowollik, C.; Wenzel, W.; Kappes, M. M.; Mayor, M. *J. Am. Chem. Soc.* **2011**, *133*, 652−655.
(69) Enyashin, A. N.; Gemming, S.; Seifert, G. *Nanotechnology* **2007**, *18*, 245702.
(70) Xiao, Z.; Wang, X.; Xu, X.; Zhang, H.; Li, Y.; Wang, Y. *J. Phys. Chem. C* **2011**, *115*, 21546−21558.